Colloids and Surfaces B: Biointerfaces 145 (2016) 72–78

Contents lists available at ScienceDirect

Colloids and Surfaces B: Biointerfaces

journal homepage: www.elsevier.com/locate/colsurfb

Single cell migration dynamics mediated by geometric confinement

Hua Zhang[a], Ruixia Hou[a], Peng Xiao[a], Rubo Xing[b], Tao Chen[a], Yanchun Han[b], Penggang Ren[c], Jun Fu[a,*]

[a] Cixi Institute of Biomedical Engineering, Ningbo Institute of Materials Technology and Engineering, Chinese Academy of Science, Ningbo 315201, China
[b] State Key Laboratory of Polymer Physics and Chemistry, Changchun Institute of Applied Chemistry, Chinese Academy of Sciences, Changchun 130022, China
[c] Institute of Printing and Packaging Engineering, Xi'an University of Technology, Xi'an 710048, China

ARTICLE INFO

Article history:
Received 1 February 2016
Received in revised form 4 April 2016
Accepted 19 April 2016
Available online 22 April 2016

Keywords:
Graphene oxide micropatterns
Osteoblasts
Cell migration
Cytoskeleton contractility

ABSTRACT

The migration dynamics of cells plays a key role in tissue engineering and regenerative medicine. Previous studies mostly focus on regulating stem cell fate and phenotype by biophysical cues. In contrast, less is known about how the geometric cues mediate the migration dynamics of cells. Here, we fabricate graphene oxide (GO) microstripes on cell non-adhesive PEG substrate by using micromolding in capillary (MIMIC) method. Such micropatterns with alternating cell adhesion and cell resistance enable an effective control of selective adhesion and migration of single cells. The sharp contrast in cell adhesion minimizes the invasion of cells into the PEG patterns, and thereby strongly confines the cells on GO microstripes. As a result, the cells are forced to adapt highly polarized, elongated, and oriented geometry to fit the patterns. A series of pattern widths have been fabricated to modulate the extent of cell deformation and polarization. Under strong confinement, the cytoskeleton contractility, intracellular traction, and actin filament elongation are highly promoted, which result in enhanced cell migration along the patterns. This work provides an important insight into developing combinatorial graphene-based patterns for the control of cell migration dynamics, which is of great significance for tissue engineering and regenerative medicine.

1. Introduction

The migration and differentiation of cells are critical procedures for tissue engineering and regenerative medicine. Recently, most efforts have been focused on the regulation of cell fate by manipulating the biophysical or biochemical cues [1–5]. Chemical cues, including ligands, ECM proteins, and biomolecules have been widely demonstrated to modulate cell behavior on chemically modified surfaces [6–8]. On the other hand, physical cues, including geometry, stiffness, topography, and stress relaxation, have showed significant influences on the adsorption and distribution of integrin ECM receptors and thereby the cellular processes through changes in cell shape and actin cytoskeleton [9–11]. In contrast, less light has been shed to the manipulation on the dynamics of cells despite of its significance on the development and regeneration of tissues. A major challenge is the difficulties in the deconvolution of random transient deformation, intracellular traction, and migration dynamics of cells. Thus, it is not clear how the cell-material interactions affect the cell geometry, intracellular traction, and skeleton traction, which are critical for the migration.

Cell growth, proliferation, and differentiation are dynamic procedures. The cytoskeleton, which interacts with substrate materials, defines the cell geometry as a result of cell-material interactions [12–14] and plays key roles in the dynamics and even fate of cells [3,15,16]. Therefore, attempts to exert geometric confinement to cells have been reported to investigate the effect of morphological cues on the behavior of cells [17–19]. The cell geometry is largely mediated by traction forces, focus adhesion area, and actomyosin contractility etc. through cellular proteins such as integrin adhesions, Rho activation, actomyosin, and focal adhesion kinase etc. [19–21]. Cells confined on nanostripes or microstripes are usually forced into highly elongated geometry [22,23]. Therein, the F-actin and myosin are activated and aligned along the patterns, which creates high cytoskeleton tension. Although the differentiation (or fate) of cells on well-designed materials has been widely investigated [4,5], little is known about how the confinement influences the morphology, intracellular traction, and thereby the migration and dynamics of cells. These issues are of particular significance as the cell migration and cytoskeleton tension is inductive during cell differentiation [24,25].

* Corresponding author.
E-mail address: fujun@nimte.ac.cn (J. Fu).

http://dx.doi.org/10.1016/j.colsurfb.2016.04.039
0927-7765/

Graphene-based micropatterns have been extensively employed to mediate cell morphology as well as adhesion, proliferation, and differentiation. For example, graphene nanogrids have showed high actin cytoskeleton proliferations coinciding with the patterns of nanogrids and accelerated osteogenic differentiation of mesenchymal stem cells (MSCs) [26]. MSCs cultured on graphene microchannels, graphene nanoribbons and rolled graphene foams aligned along the pattern length resulted in promoted neurogenesis [27–29]. Those studies mostly focus on regulating the MSCs fate and phenotype by biophysical graphene cues, while less is known about how the geometric cues mediate the migration dynamics of cells, especially when cells are strongly confined on graphene-based micropatterns with a non-fouling background.

In this study we succeeded in manipulating the deformation, orientation, and alignment of cells to mediate the intracellular contractility and cell-material interactions, and investigated the migration dynamics of such highly polarized cells. Regulated cell morphology, orientation, and alignment are well controlled by confining cells on graphene oxide (GO) micropatterns on polyethylene glycol (PEG) substrates. PEG is widely known as cell non-adhesive substrate. In contrast, GO are able to adsorb proteins and other biomolecules through specific interactions (such as π-π interaction and hydrogen bonding, etc.) with conjugated carbon ring structures and functional groups including carboxylic, epoxy, and hydroxide groups, and thus support cell attachment, growth, and differentiation [30–33]. Herein, we utilize the sharp contrast in cell adhesion on GO and on PEG to strictly confine cell seeding, adhesion, and growth. As the GO micropattern dimension is less or comparable to cell size, such a strict confinement will force the cells to adopt elongated geometry to accommodate on the stripes. By controlling the pattern width, it is convenient to manipulate the extension of cell elongation and alignment, and thus the intracellular tension and contractility. It is demonstrated that such a simple manipulation in confinement enables systematic investigation on the morphological cues to mediate the migration dynamics of single cells.

2. Materials and methods

2.1. Materials

Poly(ethylene glycol) diacrylate (PEGDA) (M_W = 547 g/mol), 2-hydroxy-4′(2-hydroxyethoxy)-2-methylpropiophenone (D2959), graphite powders (universal grade, 10000 mesh, 99.9995%) were purchased from Aladdin-Reagent China (Shanghai) Co., Ltd. Soft polydimethylsiloxane (PDMS) stamps were fabricated from Sylgard 184 (the ratio between component A and B was 1:10) on a negative silicon master (line patterns with 50 μm height and four different widths: 5 μm, 10 μm, 20 μm, and 50 μm). Other reagents and solvents were analytical reagent grade and used as received from Sinopharm Chemical Reagent unless otherwise specified.

2.2. Synthesis of graphene oxide

Graphene oxide (GO) was synthesized by using a modified Hummers method [34]. Briefly, 5 g expanded graphite powders were mixed with 5 g $NaNO_3$ and 150 mL concentrated H_2SO_4 with stirring in an ice-water bath for 4 h. Then, 15 g $KMnO_4$ was gradually added with stirring at 25 °C to obtain a highly viscous liquid. After adding deionized water (approximately 700 mL), the suspension was heated at 98 °C for 15 min. Then, the suspension was sequentially treated with warm water and H_2O_2, followed by washing with HCl and water, and freeze-drying at −70 °C for 24 h in vacuum. Finally, the obtained powders were sonicated to get stable GO aqueous suspension.

2.3. Characterization of GO nanosheets and micropatterns

Atomic force microscopy (AFM, CSPM 5500, Beijing Nano-Instruments, Ltd., China) was operated in tapping mode using silicon cantilevers (spring constant: 3–40 N m^{-1}, resonant frequency: 75–300 kHz). Optical micrographs were obtained by optical microscopy (OPM) (Olympus BX51, Japan) in the reflection mode. Static contact angles were measured on a Dataphysics OCA20 contact-angle system equipped with a bright-field optical microscope at ambient temperature. The average contact angle was obtained by measuring more than four different positions of the same substrate. X-ray photoelectron spectroscopy (XPS) (AXIS ULTRA DLD, Kratos Analytical Ltd., Manchester, UK) was carried out by using an equipment with a monochromatic Al Kα source at 10^{-9} to 10^{-8} mbar. All peaks are referenced to the signature of C 1s peak for carbon at 284.8 eV.

2.4. Fabrication of GO micropatterns on PEG substrate

Crosslinked PEG substrates were fabricated by polymerizing PEGDA via ultraviolet irradiation with D2959 as initiator. The PDMS stamps were placed in tight contact with the PEG substrate. A drop of GO suspension (2.0 mg/mL) was cast at the open channels of PDMS stamp, allowing the suspension to flow into the channel as driven by capillary force. The solvent slowly evaporated at 40 °C for 1 h. Finally, the PDMS stamp was carefully peeled off.

2.5. Cell culture and seeding

Human SV40 osteoblasts (hFOB 1.19, Shanghai Institute of Life Sciences, Cell Resource Center, Chinese Academy of Sciences) were maintained in low-glucose Dulbecco's modified Eagle medium (DMEM F12, Gibco) supplemented with 10% fetal bovine serum (FBS, Gibco), 100 U/mL penicillin, and 100 μg/mL streptomycin under a humidified atmosphere of 5% CO_2 at 37 °C. The culture medium was replaced every other day. The cells were passaged by trypsinization. Cells at passage 3, without dedifferentiation, were used for this study.

The GO micropatterned PEG substrates were sterilized in 75% ethanol for 10 min, followed by multiple washing in sterile phosphate buffered saline (PBS, pH 7.4) before cell seeding. PEG gels with GO micropatterns were then placed in a 6-well culture plate. Osteoblasts were trypsinized and seeded into the wells at a density of 4×10^4 cells mL^{-1} and incubated at 37 °C and 5% CO_2 humidified atmosphere. The cells were fixed for immunostaining after 12 h culture.

2.6. In situ tracking of osteoblast migration

The osteoblasts were seeded at a density of 2×10^3 cells mL^{-1} in order to obtain single cell adhesion on substrates. After 8 h incubation in DMEM/10% FBS, the cell migration was in situ monitored by using a time-lapse phase-contrast microscope (IX71, Olympus, Tokyo, Japan) equipped with an incubation chamber (at 37 °C and 5% CO_2 humidified atmosphere) over 12 h. The osteoblast trajectories were reconstructed based on the center positions of individual cells over time. The total cell displacement was measured by using ToupTek ToupView software every 30 min over 12 h observation. At least 15 cells were counted for calculations for each sample.

2.7. Fluorescent staining of cell cytoskeleton and nuclei

Samples with osteoblasts were removed from the culture media after 12 h incubation and carefully rinsed three times with phosphate buffer saline (PBS), and then fixed with 2.5% glutaraldehyde in PBS for 12 h. All samples were rinsed three times with PBS,

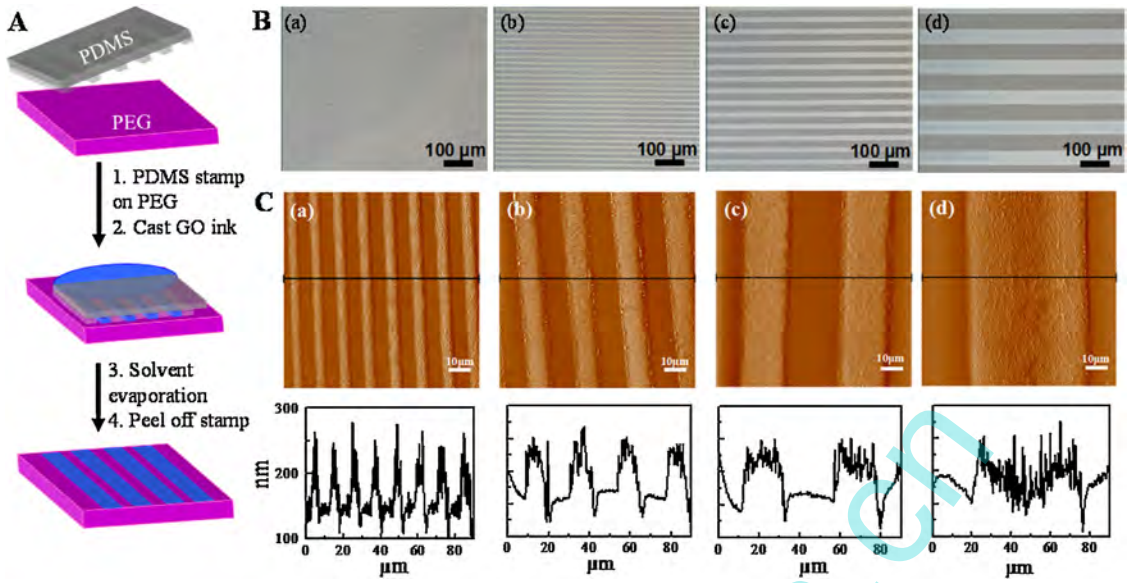

Fig. 1. (A) Schematic illustration to the micromolding in capillary (MIMC) of GO micropatterns on a PEG substrate. (B) Optical and (C) tapping mode AFM height images of GO patterns (bright) with (a) 5 μm, (b) 10 μm, (c) 20 μm, and (d) 50 μm width on PEG substrates, together with the line scan profiles.

permeabilized with 0.1% Triton X-100 in PBS for 10 min at room temperature, and then rinsed with PBS again. The osteoblasts were further blocked with 1% bovine serum albumin (BSA) in PBS for 30 min, followed by staining with 10 μg/mL phalloidin-FITC (Invitrogen) solution at 37 °C for 1 h to label the F-actin. The unbound phalloidin conjugate was removed by triplicate rinsing with PBS. 10 μg/mL 4,6-diamidino-2-phenylindole (DAPI, Invitrogen) was added and incubated in dark at 37 °C for 15 min to stain nuclei, followed by three washes in PBS. Finally, the cytoskeletons and nuclei of osteoblasts were imaged by using a confocal laser scanning microscope (CLSM, Leica TCSSP5 II, Braunschweig, Germany).

2.8. Statistical analysis

The sizes of cytoskeleton and nucleus after staining were measured by dealing with micrographs of at least 20 spreading cells using software ToupTek ToupView. All data were analyzed by *t*-test and expressed as mean ± standard deviation (SD). The statistical significance between groups was set as $p < 0.05$.

3. Results and discussion

3.1. Characterization of GO micropatterns fabricated on PEG substrate

The PEG substrate was synthesized by UV irradiation polymerization of oligo(ethylene glycol) diacrylate (*o*EGDA) ($M_W = 547$) with the presence of 2-hydroxy-4′-(2-hydroxyethoxy)-2-methylpropiophenone as initiator. Highly exfoliated graphene oxide (GO) was prepared by using a modified Hummers' method [34]. The obtained GO nanosheets possess a thickness of 1.2 nm according to atomic force microscopy (Fig. S1, Supporting information). The GO nanosheets are well dispersed in water over months, and used as *ink* for micromolding in capillary (MIMIC). The GO ink was cast on one side of the contacting polydimethylsiloxane (PDMS) stamp/PEG assembly and flowed into the microchannels as driven by capillary force (Fig. 1A). Well defined GO micropatterns with sharp edges were obtained on PEG substrate after water evaporation (Fig. 1B, C), with pattern width of 5, 10, 20, and 50 μm. The GO pattern thickness could be controlled by adjusting the GO concentration. Typically, a 2 mg mL^{-1} GO dispersion was used, resulting in a pattern thickness about 50 nm for all the patterns (Fig. 1C). The pattern surface was wrinkled with a roughness of 12.8 nm, probably formed during water evaporation (Fig. S2, Supporting information). Such wrinkles and ripples are advantageous for protein adsorption due to the high surface area, which is favorable for cell adhesion, proliferation, and differentiation [31,35]. Additionally, the static water contact angle of GO film was measured to be 36.22 ± 1.5° (Fig. S3a, Supporting information). The O/C atomic ratios of GO surface were ~0.42 (Fig. S3b, Supporting information). Such GO surface states in previous papers effectively enable proteins and growth factor adsorption and accelerate cell attachment and proliferation [36]. The GO patterns were stable on PEG substrate and did not detach during cell culture and rinsing.

3.2. Osteoblast morphology on GO micropatterns

Human SV40 osteoblasts were used as model cells for the adhesion and migration study. In order to investigate the geometric confinement on the adhesion and migration of cells, the osteoblasts were seeded at a density of 4×10^4 cells mL^{-1} on sterilized flat GO film and GO micropatterns on PEG substrates. Representative CLSM images are shown in Fig. 2. On the flat GO film, the osteoblasts appeared polygonal and spread randomly. The actin filaments are densely assembled in the cytoskeletons. Lamellipodia and filopodia extend from the leading edges of cells and anchor the cells on the GO substrate through mature focal adhesions. The average aspect ratio (AR) of cytoskeletons is 2, while the nuclei remain round shape with an average AR near 1 (Fig. 2a, j). Cells initiate the migration cycle by polarizing and extending protrusions of membrane. The protrusions comprise large, broad lamellipodia, spike like filopodia or both, and are driven by the polymerization of actin filaments. Protrusions are then stabilized by adhesions that link the actin cytoskeleton to the underlying ECM proteins, while actomysosin contraction generates traction forces on the substratum and promotes the disassembly of adhesions at the cell rear to allow the cell to move forward [37,38]. The cytoskeletons and protrusions play critical roles on the dynamics of cells. Hereafter, the cytoskeleton and protrusion morphologies are manipulated by confining osteoblasts on GO micropatterns, in order to investigate the effect of cytoskeleton elongation on the traction forces, contraction, and migration dynamics of cells.

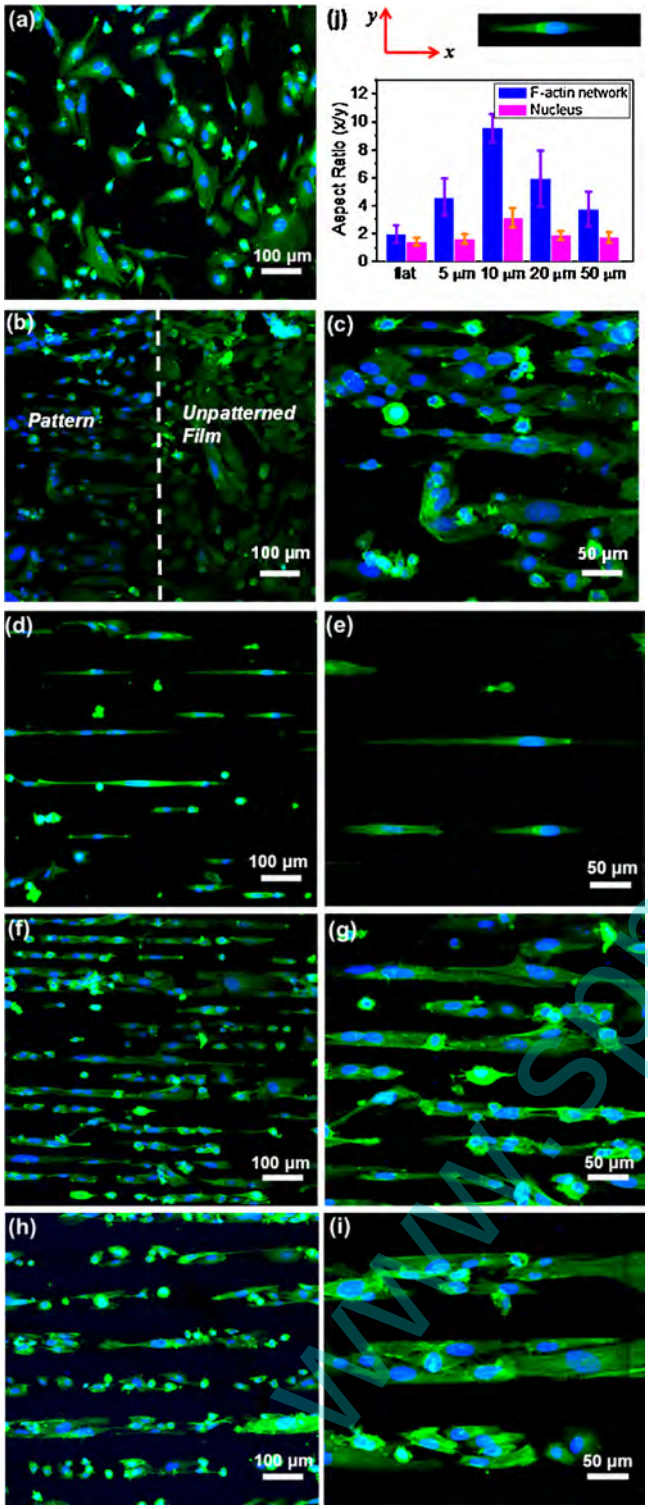

Fig. 2. Fluorescent images of osteoblasts on (a) GO film, and GO patterns with (b,c) 5 μm, (d, e) 10 μm, (f, g) 20 μm and (h, i) 50 μm width after 12 h culture. Green: cytoskeleton stained by phalloidin-FITC, blue: nuclei stained by DAPI. (j) Average aspect ratio values of cytoskeleton and nucleus on flat GO film and GO micropatterns.

Osteoblasts adhered exclusively on GO patterns and showed highly aligned, oriented, and elongated actin filaments and filopodia. On 5 μm gratings, since the period (pattern width + spacing, 10 μm) is much smaller than the cell dimension (approximately 15–20 μm of short axis), the osteoblasts spread across a few stripes (Fig. 2b) by riding on others to bridge over the PEG gap (Fig. 2c). No focal adhesions are formed on PEG. The cells are highly aligned and elongated along the patterns, in sharp contrast to the random distribution and spreading on the unpatterned GO area of the same sample (Fig. 2b). On 10 μm GO patterns, the cell adhesion density is abruptly decreased (Fig. 2d). Single cells are highly elongated, with an average cytoskeleton length of 90 μm, and very narrow lamellipodia and little filopodia on the stripe (Fig. 2e). Meanwhile, the nuclei are deformed. The average AR values of cytoskeletons and nuclei are drastically increased to 9 and 3 (Fig. 2j). Such a strong confinement reduces the numbers of actin filaments and focal adhesion area, which may reduce cell adhesion stability and thereby cell density on the stripes.

As the stripe width is increased to 20 μm, which is very close to the cell dimension, it allows for the cells to adapt a relatively relaxed state, with wide lamellipodia and filopodia (Fig. 2f). The cell number on 20 μm stripe was significantly increased than those on 10 μm patterns. The cells communicated with each other through filopodium connection. The average ARs of cytoskeletons and nuclei are decreased to 6 and 2, respectively (Fig. 2j). As the pattern width was further increased to 50 μm, two or three cells sat aside on single stripes, showing a polarized geometry and alignment along the stripes (Fig. 2f, g). The actin fibers became more relaxed than others. The average AR of cytoskeletons and nuclei further decreased to about 4 and 1.77, a little larger than the level on flat GO film.

These results demonstrate a simple and efficient method to manipulate the cell cytoskeletal orientation, elongation, and alignment by using well defined GO patterns. The patterned surfaces can increase the actin fiber formation of cytoskeleton [39–41]. The assembly and organization of actin fibers exert dynamic contractile forces against the ECM, define the cell morphologies and nuclear shape, and regulate the cellular gene expression, adhesion, migration and differentiation [42,43]. Herein, the osteoblasts were strongly confined on GO micropatterns and their cytoskeletons were highly elongated. The oriented actin cytoskeletons are likely to greatly enhance the contractile force of oteoblasts. For single cells on 10 μm and 20 μm GO patterns, in particular, such strong contractility may play key roles in cell morphologies and migration.

3.3. Single osteoblast migration on GO micropatterns

In order to investigate the effect of GO micropatterns on cell spreading and migration, osteoblasts on 10 μm and 20 μm micropatterns after 12 h incubation were in situ traced by using a time-lapse phase-contrast microscope equipped with an incubation chamber in 5% CO_2 humidified atmosphere at 37 °C. Cells cultured on polystyrene (PS) culture plate and GO film were used as negative controls. A low cell density (2×10^3 cell mL^{-1}) was used for seeding on substrates in order to minimize cell–cell contact.

Fig. 3 shows representative optical micrographs of single cells on the PS plate (Fig. 3a), GO film (Fig. 3b) and GO micropatterns (Fig. 3c–d). On the PS plate, a transient elongated cell was sampled. In the first 120 min, its centre remained almost stationary while both ends contracted asymmetrically toward the nucleus to pull the cell forward. The cell migrated randomly through cyclic extension and contraction of lamellipodia and release of focal adhesion (Fig. 3a). The cell migration is much slower on GO film than on PS. The osteoblasts slowly and extended and weakly contracted their protrusion to pull the cell forward in 480 min (Fig. 3b). These results indicate that the F-actin has stronger interactions to GO than to PS. On GO patterned surface, in contrast, the elongated single cells slightly extended a leading edge and then rapidly contracted the rear, resulting in movements along the pattern in minutes (Fig. 3c, d). Specifically, the osteoblast contraction to round shape took 7.3 ± 1.9 min on 10 μm GO patterns and 4.1 ± 1.8 min on 20 μm GO patterns ($p < 0.05$, Fig. 3e).

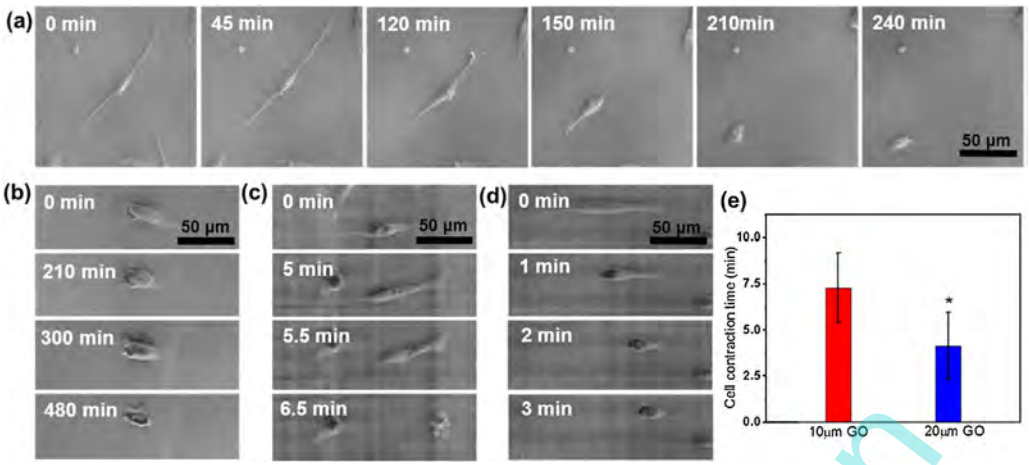

Fig. 3. Time-lapse bright field images of osteoblasts on (a) PS plate, (b) flat GO film, and GO micropatterns with (c) 10 μm and (d) 20 μm widths. (e) The contraction time of osteoblasts on 10 μm and 20 μm GO micropatterns (*$p < 0.05$, t-test).

In order to quantitatively analyze the migration of single osteoblasts, the cell migration trajectories on various substrates were recorded by using time-lapse microscopy (see movies in Supporting information). The direction parallel with the GO stripes was defined as the x- coordinate. The cell center was recorded every 30 min and plotted on a trace map (Fig. 4). On the PS plate and GO film, osteoblasts moved randomly (movie S1 for PS and S2 for GO, Supporting information). On the PS substrate, the cell trajectories covered an area of about $200 \times 70\ \mu m^2$ (Fig. 4a). The cell migration on GO film covered an area of about $15 \times 10\ \mu m^2$ (Fig. 4b). In contrast, on GO patterns, the cell migration was restricted within the GO stripes (movie S3, Supporting information), with the trajectories equally distributed in the $+x$ and $-x$ direction due to the symmetrically elongated morphology of cells (Fig. 4c, d). The trajectory distance was about 200 μm on 10 μm GO patterns (Fig. 4c), and about 80 μm on 20 μm GO patterns (Fig. 4d). These results indicate that the cell movement on GO patterns is strongly and uniaxially confined and the migration direction is dominated by the polarization of F-actins (Fig. 2).

The migration dynamics is highly related to both the cell-material interaction and intracellular contractility. Under confinement, the intracellular contractility is increased as a result of the high alignment and elongation of actin filaments. Herein, we examine the morphology evolution of cells on GO micropatterns in order to investigate the relaxation of cells on micropatterns through deformation from elongated state to round shape. The cell shape parameters including AR and spreading areas (SA) of cytoskeleton, based on in situ tracking on at least 15 cells, were used to quantitatively measure the morphology evolution of cells. The results are summarized in Fig. 5. On flat substrates, the AR of osteoblast cytoskeleton on the PS plate and GO film were almost constant (3.1 ± 1.2) during migration. In contrast, osteoblasts on 10 μm and 20 μm GO patterns relaxed from stripe to ellipse or round shape, with the AR decreased from 8.6 ± 3.0 and 5.6 ± 1.1 to 1.2 ± 0.3.

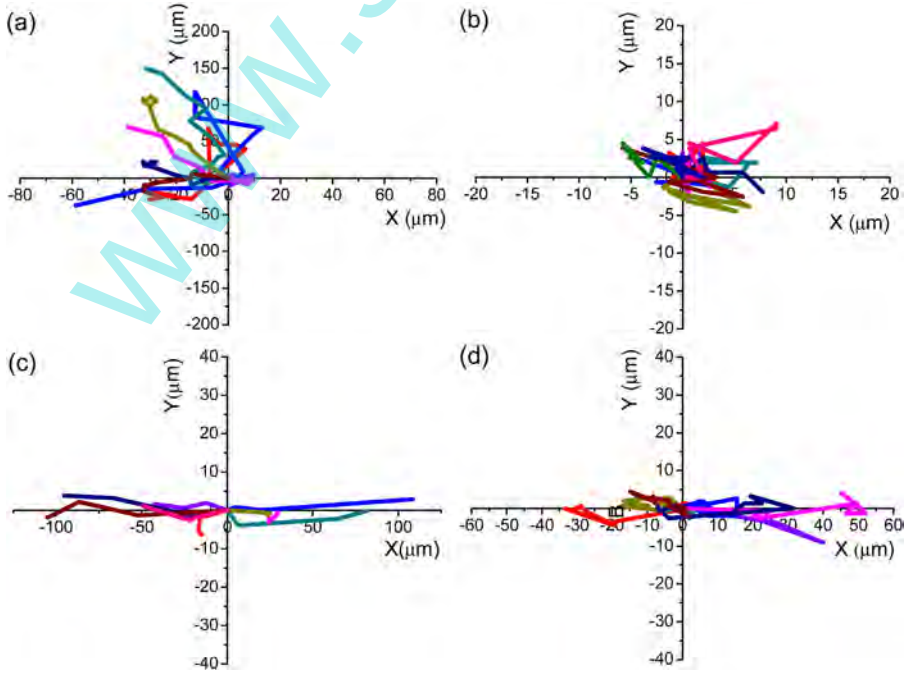

Fig. 4. Cell migration trajectories on (a) PS plate, (b) flat GO film, and GO patterns with (c) 10 μm and (d) 20 μm width. Cell motions were continuously recorded every 60 min for 12 h.

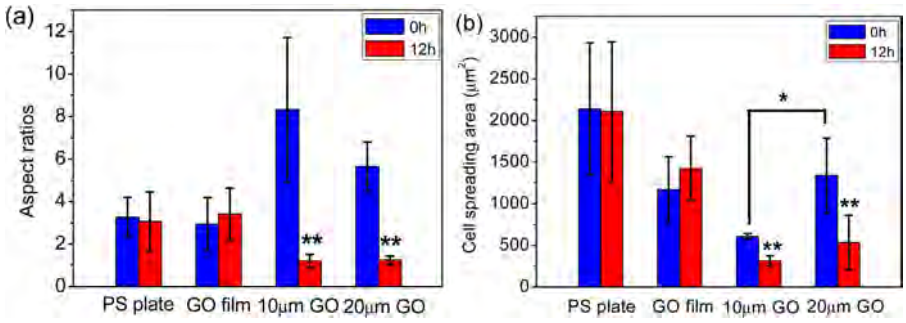

Fig. 5. Diagrams of (a) aspect ratio and (b) spreading area of cells before and after migration on different substrates (*$p < 0.05$; **$p < 0.01$, *t*-test). Error bars represent standard deviations.

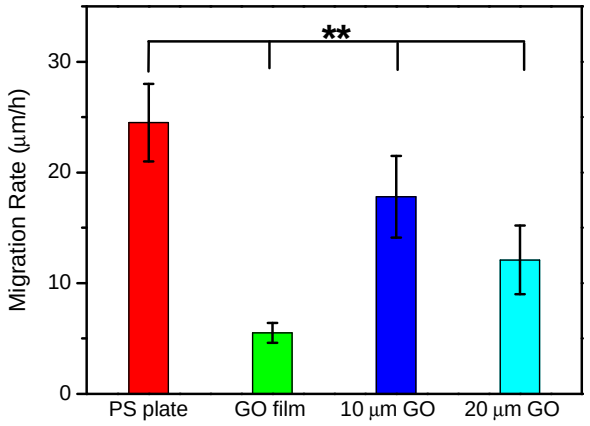

Fig. 6. The average migration rates of cells on different substrates (**$p < 0.01$). Error bars represent standard deviations.

Correspondingly, the average cell SA values on 10 and 20 μm GO patterns were decreased from $607 \pm 33\ \mu m^2$ and $1343 \pm 448\ \mu m^2$ to $315 \pm 61\ \mu m^2$ and $536 \pm 325\ \mu m^2$, while those on PS plate and GO film remained almost unchanged ($2100 \pm 800\ \mu m^2$ and $1200 \pm 400\ \mu m^2$). These results indicate that, under strong micro-confinement, the elongated osteoblasts contract their cytoskeleton through actin stress fiber reorganization to keep adhesive homeostasis. Thus, the elongated osteoblasts may actively generate strong contractile forces for cell movement, which may account for the long cell migration distance on GO micropatterns.

Such high contractile forces strongly influence the migration rate of osteoblasts. Fig. 6 compares the average cell migration rates on the 10 μm and 20 μm GO patterns, as well as those on PS plate and flat GO film, based on statistics of at least 15 spreading cells. Notably, osteoblasts on flat GO film showed a slow migration at 5.5 ± 0.9 μm/h, whereas it was fastest on PS plate (24.5 ± 3.5 μm/h). Previous studies have demonstrated that a strong adhesion of focal adhesions to substrates delays the release and migration of cells [14,44]. Herein, the osteoblasts have a strong adhesion to GO film with polar functional groups [45,46]. However, on 10 μm and 20 μm GO micropatterns, the migration rates of osteoblasts were significantly improved at 17.8 ± 3.7 μm/h and 12.1 ± 3.1 μm/h. It is likely that the high cytoskeleton tension and intracellular traction forces of the highly elongated cells may partly overcome the strong adhesion between cells and GO, leading to higher cell contractility and mobility. Moreover, the migration rate on 10 and 20 μm GO patterns were significantly different ($p < 0.01$), further indicating that the diverse cell spread morphologies generate different traction for cell motility and migration.

Why do the elongated osteoblasts on the GO micropatterns deform and migrate rapidly, even if the osteoblasts exert strong adhesive interactions on GO substrate? Typically, the migration of mammalian cells includes five steps [47,48]: (*i*) morphological polarization; (*ii*) extension of membranes toward the direction of motility by assembly of actin filaments; (*iii*) formation of attachments between the leading membranes and the substrate by integrin; (*iv*) contraction of the cell body from both ends toward the nucleus; (*v*) release of adhesion receptor from cytoskeleton and substrate at the back of the cell and recycling of adhesion receptors to the front of the cell. These processes lead to a net translocation of cell body. In this study, the GO micropatterns confine the osteoblasts to remodel F-actin elongation and to polarize cytoskeleton along GO stripes (Fig. 2). The highly polarized cells generate strong cytoskeleton traction, resulting in a rapid contraction and release within 4–7 min, while the random osteoblasts on GO film took about 6 h. Therefore, the polarized osteoblasts on GO surface mainly enhance the contractile force of cytoskeleton, which strongly forces the release of adhesion receptors at the back of cells on GO micropatterns.

4. Conclusions

In conclusion, single cell migration dynamics have been mediated by regulating the geometric confinement on cell-adhesive graphene oxide (GO) micropatterns. It is convenient and efficient to fabricate GO micropatterns with different widths on cell non-adhesive PEG substrates. Such a sharp contrast in cell adhesion enables a strong confinement of single cells on GO micropatterns. By controlling the pattern width, cells are forced to adapt highly elongated, aligned, and oriented geometries on GO patterns. With an increase in the AR values of cytoskeleton and nuclei of the osteoblasts, the actin filament alignment and elongation, cytoskeleton contractility, and intracellular traction force are highly promoted, leading to aligned attachment and oriented migration of single cells on GO micropatterns. Such highly deformed and stressed cells are forced to rapidly release the adhesion receptors within 4–7 min, in comparison to that on flat GO film for about 6 h. We conclude that the strong cell-GO interactions determine the cell migration rate on GO substrate, while the enhanced intracellular traction and cytoskeleton contractility highly accelerate the cell migration dynamics.

Conflict of interest statement

The authors declare no competing financial interest.

Acknowledgments

This study was supported by the Natural Science Foundation of China (21574145, 51273161), the Hundred Talents Program of the Chinese Academy of Sciences (JF), the Zhejiang Natural Sci-

ence Foundation of China (LR13B040001), and the Ningbo Natural Science Foundation (2015A610025).

Appendix A. Supplementary data

Supplementary data associated with this article can be found, in the online version, at http://dx.doi.org/10.1016/j.colsurfb.2016.04.039.

References

[1] N.F. Huang, E.S. Lai, A.J.S. Ribeiro, S. Pan, B.L. Pruitt, G.G. Fuller, J.P. Cooke, Spatial patterning of endothelium modulates cell morphology, adhesiveness and transcriptional signature, Biomaterials 34 (2013) 2928–2937.
[2] S. Martino, F. D'Angelo, I. Armentano, J.M. Kenny, A. Orlacchio, Stem cell-biomaterial interactions for regenerative medicine, Biotechnol. Adv. 30 (2012) 338–351.
[3] X. Yao, R. Peng, J. Ding, Cell–material interactions revealed via material techniques of surface patterning, Adv. Mater. 25 (2013) 5257–5286.
[4] W.L. Murphy, T.C. McDevitt, A.J. Engler, Materials as stem cell regulators, Nat. Mater. 13 (2014) 547–557.
[5] M.P. Lutolf, P.M. Gilbert, H.M. Blau, Designing materials to direct stem-cell fate, Nature 462 (2009) 433–441.
[6] Z.A. Cheng, O.F. Zouani, K. Glinel, A.M. Jonas, M.-C. Durrieu, Bioactive chemical nanopatterns impact human mesenchymal stem cell fate, Nano Lett. 13 (2013) 3923–3929.
[7] X. Wang, S. Li, C. Yan, P. Liu, J. Ding, Fabrication of RGD micro/nanopattern and corresponding study of stem cell differentiation, Nano Lett. 15 (2015) 1457–1467.
[8] V. Llopis-Hernandez, M. Cantini, C. González-García, M. Salmerón-Sánchez, Material-based strategies to engineer fibronectin matrices for regenerative medicine, Int. Mater. Rev. 60 (2015) 245–264.
[9] E.H. Ahn, Y. Kim, S.S. An, J. Afzal, S. Lee, M. Kwak, K.-Y. Suh, D.-H. Kim, A. Levchenko, Spatial control of adult stem cell fate using nanotopographic cues, Biomaterials 35 (2014) 2401–2410.
[10] A. Higuchi, Q.-D. Ling, Y. Chang, S.-T. Hsu, A. Umezawa, Physical cues of biomaterials guide stem cell differentiation fate, Chem. Rev. 113 (2013) 3297–3328.
[11] K. Kolind, K.W. Leong, F. Besenbacher, M. Foss, Guidance of stem cell fate on 2D patterned surfaces, Biomaterials 33 (2012) 6626–6633.
[12] Q.Y. Tang, W.X. Qian, Y.H. Xu, S. Gopalakrishnan, J.Q. Wang, Y.W. Lam, S.W. Pang, Control of cell migration direction by inducing cell shape asymmetry with patterned topography, J. Biomed. Mater. Res. A 103 (2015) 2383–2393.
[13] L. Han, Z. Mao, J. Wu, Y. Guo, T. Ren, C. Gao, Unidirectional migration of single smooth muscle cells under the synergetic effects of gradient swelling cue and parallel groove patterns, Coll. Surf., B 111 (2013) 1–6.
[14] J. Wu, Z. Mao, C. Gao, Controlling the migration behaviors of vascular smooth muscle cells by methoxy poly (ethylene glycol) brushes of different molecular weight and density, Biomaterials 33 (2012) 810–820.
[15] K.M. Schultz, K.A. Kyburz, K.S. Anseth, Measuring dynamic cell–material interactions and remodeling during 3D human mesenchymal stem cell migration in hydrogels, Proc. Natl. Acad. Sci. 112 (2015) E3757–E3764.
[16] H.S. Dhowre, S. Rajput, N.A. Russell, M. Zelzer, Responsive cell-material interfaces, Nanomedicine 10 (2015) 849–871.
[17] W. Zhang, G. Wang, Y. Liu, X. Zhao, D. Zou, C. Zhu, Y. Jin, Q. Huang, J. Sun, X. Liu, The synergistic effect of hierarchical micro/nano-topography and bioactive ions for enhanced osseointegration, Biomaterials 34 (2013) 3184–3195.
[18] J.E. Samorezov, C.M. Morlock, E. Alsberg, Dual ionic and photo-crosslinked alginate hydrogels for micropatterned spatial control of material properties and cell behavior, Bioconjugate Chem. (2015).
[19] J.M. Jang, S.-H.-T. Tran, S.C. Na, N.L. Jeon, Engineering controllable architecture in Matrigel for 3D cell alignment, ACS Appl. Mater. Interfaces 7 (2015) 2183–2188.
[20] T. Kobayashi, M. Sokabe, Sensing substrate rigidity by mechanosensitive ion channels with stress fibers and focal adhesions, Curr. Opin. Cell Biol. 22 (2010) 669–676.
[21] J. Lee, A.A. Abdeen, X. Tang, T.A. Saif, K.A. Kilian, Geometric guidance of integrin mediated traction stress during stem cell differentiation, Biomaterials 69 (2015) 174–183.
[22] X. Shi, T. Fujie, A. Saito, S. Takeoka, Y. Hou, Y. Shu, M. Chen, H. Wu, A. Khademhosseini, Periosteum-mimetic structures made from freestanding microgrooved nanosheets, Adv. Mater. 26 (2014) 3290–3296.
[23] S. Singh, S.B. Bandini, P.E. Donnelly, J. Schwartz, J.E. Schwarzbauer, A cell-assembled, spatially aligned extracellular matrix to promote directed tissue development, J. Mater. Chem. B 2 (2014) 1449–1453.
[24] S. Khetan, M. Guvendiren, W.R. Legant, D.M. Cohen, C.S. Chen, J.A. Burdick, Degradation-mediated cellular traction directs stem cell fate in covalently crosslinked three-dimensional hydrogels, Nat. Mater. 12 (2013) 458–465.
[25] N. Huebsch, P.R. Arany, A.S. Mao, D. Shvartsman, O.A. Ali, S.A. Bencherif, J. Rivera-Feliciano, D.J. Mooney, Harnessing traction-mediated manipulation of the cell/matrix interface to control stem-cell fate, Nat. Mater. 9 (2010) 518–526.
[26] O. Akhavan, E. Ghaderi, M. Shahsavar, Graphene nanogrids for selective and fast osteogenic differentiation of human mesenchymal stem cells, Carbon 59 (2013) 200–211.
[27] O. Akhavan, E. Ghaderi, The use of graphene in the self-organized differentiation of human neural stem cells into neurons under pulsed laser stimulation, J. Mater. Chem. B 2 (2014) 5602–5611.
[28] O. Akhavan, E. Ghaderi, Differentiation of human neural stem cells into neural networks on graphene nanogrids, J. Mater. Chem. B 1 (2013) 6291–6301.
[29] O. Akhavan, E. Ghaderi, S.A. Shirazian, R. Rahighi, Rolled graphene oxide foams as three-dimensional scaffolds for growth of neural fibers using electrical stimulation of stem cells, Carbon 97 (2016) 71–77.
[30] W.C. Lee, C.H.Y. Lim, H. Shi, L.A. Tang, Y. Wang, C.T. Lim, K.P. Loh, Origin of enhanced stem cell growth and differentiation on graphene and graphene oxide, ACS Nano 5 (2011) 7334–7341.
[31] T.R. Nayak, H. Andersen, V.S. Makam, C. Khaw, S. Bae, X. Xu, P.-L.R. Ee, J.-H. Ahn, B.H. Hong, G. Pastorin, Graphene for controlled and accelerated osteogenic differentiation of human mesenchymal stem cells, ACS Nano 5 (2011) 4670–4678.
[32] O. Chaudhuri, L. Gu, D. Klumpers, M. Darnell, S.A. Bencherif, J.C. Weaver, N. Huebsch, H.-p. Lee, E. Lippens, G.N. Duda, Hydrogels with tunable stress relaxation regulate stem cell fate and activity, Nat. Mater. (2015).
[33] T.-H. Kim, S. Shah, L. Yang, P.T. Yin, M.K. Hossain, B. Conley, J.-W. Choi, K.-B. Lee, Controlling differentiation of adipose-derived stem cells using combinatorial graphene hybrid-pattern arrays, ACS Nano 9 (2015) 3780–3790.
[34] P.-G. Ren, D.-X. Yan, X. Ji, T. Chen, Z.-M. Li, Temperature dependence of graphene oxide reduced by hydrazine hydrate, Nanotechnology 22 (2011) 055705.
[35] N. Li, Q. Zhang, S. Gao, Q. Song, R. Huang, L. Wang, L. Liu, J. Dai, M. Tang, G. Cheng, Three-dimensional graphene foam as a biocompatible and conductive scaffold for neural stem cells, Sci. Rep. 3 (2013).
[36] X. Shi, H. Chang, S. Chen, C. Lai, A. Khademhosseini, H. Wu, Regulating cellular behavior on few-layer reduced graphene oxide films with well-controlled reduction states, Adv. Funct. Mater. 22 (2012) 751–759.
[37] J.T. Parsons, A.R. Horwitz, M.A. Schwartz, Cell adhesion: integrating cytoskeletal dynamics and cellular tension, Nat. Rev. Mol. Cell Biol. 11 (2010) 633–643.
[38] S.L. Gupton, C.M. Waterman-Storer, Spatiotemporal feedback between actomyosin and focal-adhesion systems optimizes rapid cell migration, Cell 125 (2006) 1361–1374.
[39] M.J. Dalby, D. McCloy, M. Robertson, C.D.W. Wilkinson, R.O.C. Oreffo, Osteoprogenitor response to defined topographies with nanoscale depths, Biomaterials 27 (2006) 1306–1315.
[40] M.J. Dalby, D. McCloy, M. Robertson, H. Agheli, D. Sutherland, S. Affrossman, R.O.C. Oreffo, Osteoprogenitor response to semi-ordered and random nanotopographies, Biomaterials 27 (2006) 2980–2987.
[41] Z.A. Cheng, O.F. Zouani, K. Glinel, A.M. Jonas, M.C. Durrieu, Bioactive chemical nanopatterns impact human mesenchymal stem cell fate, Nano Lett. 13 (2013) 3923–3929.
[42] O. Du Roure, A. Saez, A. Buguin, R.H. Austin, P. Chavrier, P. Siberzan, B. Ladoux, Force mapping in epithelial cell migration, Proc. Natl. Acad. Sci. U.S.A. 102 (2005) 2390–2395.
[43] C. Le Clainche, M.-F. Carlier, Regulation of actin assembly associated with protrusion and adhesion in cell migration, Physiol. Rev. 88 (2008) 489–513.
[44] A. Pathak, S. Kumar, Independent regulation of tumor cell migration by matrix stiffness and confinement, Proc. Natl. Acad. Sci. 109 (2012) 10334–10339.
[45] D. Depan, B. Girase, J. Shah, R. Misra, Structure–process–property relationship of the polar graphene oxide-mediated cellular response and stimulated growth of osteoblasts on hybrid chitosan network structure nanocomposite scaffolds, Acta Biomater. 7 (2011) 3432–3445.
[46] S.H. Ku, C.B. Park, Myoblast differentiation on graphene oxide, Biomaterials 34 (2013) 2017–2023.
[47] M.P. Sheetz, D. Felsenfeld, C. Galbraith, D. Choquet, Cell migration as a five-step cycle, Biochem. Soc. Symp. 65 (1998) 233–243.
[48] X. Jiang, D.A. Bruzewicz, A.P. Wong, M. Piel, G.M. Whitesides, Directing cell migration with asymmetric micropatterns, Proc. Natl. Acad. Sci. U.S.A. 102 (2005) 975–978.